Longitudinal current losses in rf linear accelerators

Nathan Brown[*] and Martin Reiser
Institute for Plasma Research, University of Maryland, College Park, Maryland 20742
(Received 21 August 1995; revised manuscript received 26 April 1996)

The effective longitudinal focusing force of the radio-frequency (rf) field in an rf linear accelerator (linac) allows for the loss of particles due to the natural tail on the thermal equilibrium distribution. Equations are derived and numerical results are presented for the resulting fractional loss rate of particles from the rf bucket. This loss rate represents the best possible case. Existing accelerators have beams that are not in thermal equilibrium. Equipartitioning, mismatch, and phase oscillations, effects that are not treated here, can lead to emittance growth, the formation of nonthermal tails (halos), and greater particle losses. [S1063-651X(96)06009-6]

PACS number(s): 41.85.Ew, 29.27.Eg, 52.25.Wz

I. INTRODUCTION

Radio-frequency (rf) linear accelerators for applications such as heavy ion inertial fusion, high energy colliders, tritium production, and the transmutation of radioactive nuclear waste require beam currents that are high enough that space-charge forces play a significant role in the beam evolution and equilibrium properties. Nonlinear or oscillating space-charge forces have been shown to result in tails or halos on the transverse particle distribution [1–4]. At high enough energies, particle losses into the conducting channel can cause radioactivity, inhibiting routine maintenance. Fractional particle losses as small as 10^{-8} per meter have been predicted to cause radioactivity in the accelerators proposed for radioactive waste transmutation [5]. The formation and existence of transverse halos [1–3] and transverse thermal tails [4] in high-current beams have been studied in order to predict the particle losses resulting from nonlinear forces and from oscillations due to mismatch in the transverse direction. Here we consider particle losses in the longitudinal direction in an rf field, which can also lead to current losses into the conducting channel in high-current linacs.

The effective external focusing field of an rf accelerating and focusing wave is nonlinear and drops off after a certain distance in the trailing end of each bunch [6]. Particles moving backward from the trailing end of a bunch can leak out of the region of phase in the rf wave in which the bunch can be contained (the rf bucket), and due to coupling between the longitudinal and transverse forces, they can then become lost into the conducting channel. A bunch with an anisotropic temperature or a nonequilibrium density profile will relax toward a thermal equilibrium distribution, which has a natural tail in the longitudinal direction. This tail will lead to the loss of particles from the rf bucket. Thermal equilibria have been found previously for a bunched beam with linear external focusing forces [4,7]. The method used in Ref. [4] is used in Sec. II with the inclusion of nonlinearities in the focusing in the rf bucket. In Sec. III, equations are derived and numerical results are presented for the fractional current loss rate from the thermal equilibrium distribution.

The bunched beams in existing linear accelerators are generally not in thermal equilibrium. The ratio of the transverse to longitudinal focusing force constants is increased as the beam propagates along the channel in order to reduce current losses in the transverse direction, and as a result the transverse and longitudinal temperatures are not equal. The relaxation of an anisotropic temperature leads to emittance growth [8] and the formation of nonthermal tails (halos) on the distribution, which can lead to further particle losses in both the transverse and longitudinal directions. The particle loss rates that are found here represent a best-case scenario, in which each bunch is in thermal equilibrium in the external focusing field, and is free from oscillations in the phase and in the bunch length. An accelerator with a bunched beam that is maintained near thermal equilibrium has recently been proposed [9].

II. THERMAL EQUILIBRIUM

The thermal equilibrium line charge density with linear external focusing forces has a parabolic shape at zero temperature, and a Gaussian shape in the limit of high temperature. For finite, nonzero temperatures the shape is determined numerically by combining the Boltzmann relation with the Poisson equation,

$$\nabla^2 \phi_s(\vec{r}) = -\frac{q}{\epsilon_0} n(\vec{r}) = -\frac{q}{\epsilon_0} n(0) \exp\left(-\frac{q[\phi(\vec{r})-\phi(0)]}{k_B T}\right),$$
(1)

where ϕ_s is the self-potential including images, $\vec{r}$ is position, q is the particle charge, ϵ_0 is the permittivity of free space, $\phi(\vec{r})$ is the total potential (self and external focusing), k_B is Boltzmann's constant, and T is the temperature.

The effective external focusing potential on the axis in the rf field in cylindrical coordinates (r,z) is [6]

$$\phi_e(r=0,z) = \frac{E_m v_0}{\omega_{rf}}\left[\sin\left(\varphi_0 - \frac{\omega_{rf}z}{v_0}\right) - \sin(\varphi_0)\right.$$

$$\left. + \frac{\omega_{rf}z}{v_0}\cos(\varphi_0)\right],$$
(2)

*Present address: G. H. Gillespie Associates, Inc., P.O. Box 2961, Del Mar, CA 92014.
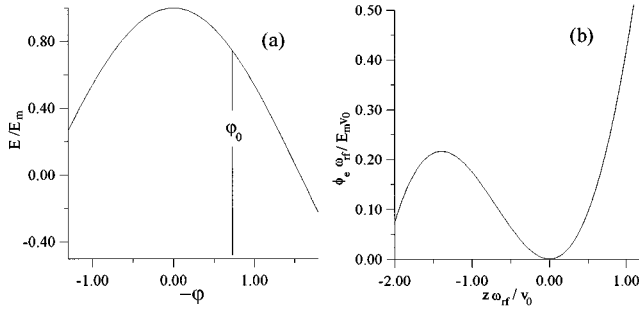
FIG. 1. The rf electric field (a) and the effective focusing potential on the axis of the rf field (b) for $\varphi_0 = -40°$.

where E_m is the peak rf electric field, ω_{rf} is the frequency of the rf field, v_0 is the beam velocity (the velocity of the synchronous particle in the lab frame), and φ_0 is the synchronous phase. When the bunch size is much smaller than the rf bucket, this is approximately a quadratic potential with a linear focusing force, centered at $z=0$. The rf electric field and the effective focusing potential on the axis are shown in Fig. 1 for a synchronous phase of $\varphi_0 = -40°$. A more detailed description of the longitudinal focusing and a derivation of Eq. (2) can be found in Ref. [6]. For the bunch to be close to equilibrium with an external focusing potential that allows some current to be lost, it is assumed that in the time scales of interest the fractional particle loss is small enough that the equilibrium of the remaining particles is not significantly affected by the losses.

An approximation for the rf focusing field off the axis is found by transforming the potential of Eq. (2) into the beam frame, expanding in even powers of r and solving for the coefficients from Laplace's equation [10]. The result describes the rf focusing in the beam frame, in which the rf field has no magnetic component. In the laboratory frame the rf field has a magnetic component that results in a transverse force; this force, however, can be included in an effective electrostatic potential in the laboratory frame provided that the particle velocities are nonrelativistic in the beam frame.

Magnetic lenses (solenoids or quadrupoles) provide a transverse external focusing force that is approximated as continuous along the channel (independent of z) and linear in radius in cylindrical coordinates. The potential for this force is written as $\phi_{\perp e} = \frac{1}{2}\gamma_0 m v_0^2 k_{x0}^2 r^2 q$, where m is the particle mass, $\gamma_0 = (1 - v_0^2/c^2)^{-1/2}$ is the relativistic factor, c is the speed of light, and k_{x0} is the transverse focusing wave constant. The resulting effective electrostatic potential in the laboratory frame is

$$
\phi_e(r,z) \approx \frac{1}{2}\gamma_0 m v_0^2 k_{x0}^2 r^2 q + \frac{E_m v_0}{\omega_{rf}}\left[\sin\left(\varphi_0 - \frac{\omega_{rf}z}{v_0}\right) - \sin(\varphi_0)\right.
$$

$$
+ \frac{\omega_{rf}z}{v_0}\cos(\varphi_0)\left] + \frac{E_m v_0}{\omega_{rf}}\sin\left(\varphi_0 - \frac{\omega_{rf}z}{v_0}\right)\right.
$$

$$
\times\left[\frac{1}{4}\left(\frac{\omega_{rf}r}{\gamma_0 v_0}\right)^2 + \frac{1}{64}\left(\frac{\omega_{rf}r}{\gamma_0 v_0}\right)^4 + \frac{1}{2304}\left(\frac{\omega_{rf}r}{\gamma_0 v_0}\right)^6\right],
$$

(3)

in which the expansion in r for the rf field is taken up to sixth order. Since the synchronous phase φ_0 is negative, the
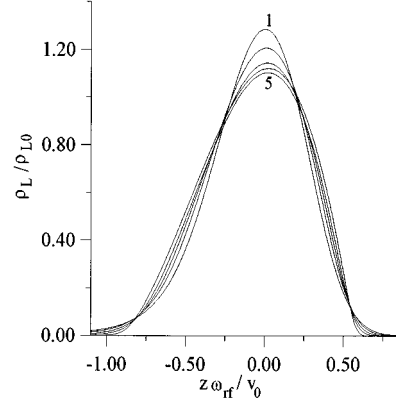
FIG. 2. Normalized line charge density profiles with a synchronous phase of $\varphi_0 = -40°$ and a phase half-width of $\Delta\varphi_m = 40°$. The profiles from 1 through 5 correspond to longitudinal space charge tune depressions of 0.95, 0.8, 0.65, 0.5, and 0.3, respectively. The aspect ratio in the beam frame is $\gamma_0 z_m/r_m = 5$.

majority of the beam is contained within the region $z > v_0\varphi_0/\omega_{rf}$, for which the transverse component of the rf field provides a defocusing force.

Figure 2 shows a set of thermal equilibrium line charge density profiles with a synchronous phase of $\varphi_0 = -40°$ and a phase half-width of $\Delta\varphi_m = 40°$. These profiles were found by Newton's method with simultaneous overrelaxation [11], as was done in Ref. [4]. Line charge densities are in units of ρ_{L0}, the line charge density at the center of the equivalent parabola, which is defined to have the same root-mean-square (rms) value for z, the same number of particles, and the same synchronous phase. The temperature of each profile is defined by the longitudinal space charge tune depression, k_z/k_{z0}, which is calculated from the envelope equation [9]. k_z and k_{z0} are, respectively, the longitudinal focusing wave constants with and without space charge; a tune depression of zero corresponds to zero temperature and a tune depression of one corresponds to the high temperature limit (negligible space charge forces).

The amplitude of the external focusing for the profiles shown in Fig. 2 is adjusted in each case in order to keep the rms value for z constant for profiles with different temperatures. The phase half-width is defined as the phase half-width of the equivalent parabolic line charge profile. The aspect ratio in the beam frame ($\gamma_0 z_m/r_m$) is 5 for the profiles of Fig. 2; $\gamma_0 z_m$ and r_m are, respectively, the half-length (in the beam frame) and peak radius of the equivalent uniform ellipsoid [4]. The profiles of Fig. 2 are similar to those with linear focusing [4,7], except for the asymmetry due to the extension of the bunch into the nonlinear regions of the effective rf focusing field. The profiles drop off more slowly in the backward direction, where current losses occur. Figure 3 shows the density profile for a bunch with an aspect ratio of $\gamma_0 z_m/r_m = 2$, a synchronous phase of $\varphi_0 = -30°$ and a phase half-width of $\Delta\varphi_m = 20°$. The longitudinal space charge tune depression is $k_z/k_{z0} = 0.4$ and the transverse space charge tune depression is $k_x/k_{x0} = 0.48$. The radius is in units of r_m, the longitudinal distance is in units of z_m, and the density is in units of n_0, the density of the equivalent uniform ellipsoid.
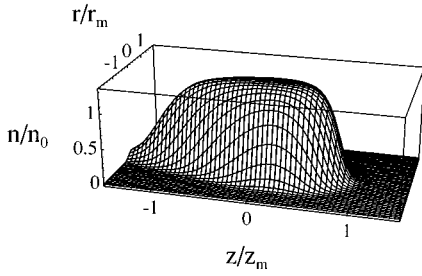
FIG. 3. Density as a function of position in cylindrical coordinates, with $\varphi_0 = -30°$, $\Delta\varphi_m = 20°$, $\gamma_0 z_m / r_m = 2$, and $k_z/k_{z0} = 0.4$.

III. CURRENT LOSSES FROM THERMAL EQUILIBRIUM

The loss of particles occurs at the local maximum in the total potential, which is slightly closer to the synchronous phase than the local maximum in the effective focusing potential in Fig. 1. The fractional particle loss per meter along the channel is found from the flux of particles due to thermal motion across this boundary. This flux is proportional to the line charge density, which is determined numerically from the thermal equilibrium profiles.

The flux of particles with density n_b and longitudinal velocity distribution $f(v_\parallel)$ across a perpendicular boundary in the beam frame is

$$\Phi = \int_0^\infty n_b v_\parallel f(v_\parallel) dv_\parallel. \tag{4}$$

With a Maxwellian velocity distribution with temperature T_b in the beam frame [12], the number of particles per unit time crossing the boundary in the beam frame is $[\rho_{Lb}(z_{lb})/q](k_B T_b/2\pi m)^{1/2}$, in which $\rho_{Lb}(z_{lb})$ is the line charge density in the beam frame at the boundary where the total electric field is zero. $\rho_L(z_l)$ is the same quantity in the laboratory frame, which is related to the beam frame line charge density by $\rho_{Lb} = \rho_L/\gamma_0$. The resulting fractional loss per unit distance along the channel in the laboratory frame is

$$f = \frac{\rho_L(z_l)}{qNv_0}\left(\frac{k_B T}{2\pi\gamma_0^3 m}\right)^{1/2}. \tag{5}$$

This can be rewritten as

$$f = \left(\frac{3}{4(10\pi)^{1/2}}\right)\left(\frac{\rho_L(z_l)}{\rho_{L0}}\right)\left(\frac{\bar{\epsilon}_{nz}}{\beta_0\gamma_0^3\bar{z}^2}\right), \tag{6}$$

where $\bar{\epsilon}_{nz} = \bar{z}(\gamma_0^3 k_B T/mc^2)^{1/2}$ is the rms normalized longitudinal emittance [6], $\bar{z}$ is the rms value for z, and $\beta_0 = v_0/c$. $\rho_L(z_l)/\rho_{L0}$, the normalized line charge density at the longitudinal position where the total electric field is zero, is determined numerically for each profile. Figure 4 shows the normalized line charge density at z_l as a function of k_z/k_{z0} for a synchronous phase of $\varphi_0 = -40°$ and phase half-widths of $\Delta\varphi_m = 20°$, $30°$, and $40°$ (lines 1, 2, and 4, respectively) and for a synchronous phase of $\varphi_0 = -30°$ and phase half-width of $\Delta\varphi_m = 20°$ (line 3).

The profiles in Fig. 4 all have an aspect ratio in the beam frame of $\gamma_0 z_m / r_m = 2$ and a pipe radius of $b = 3r_m = 3(\frac{5}{2})^{1/2}\bar{r}$ ($\bar{r}$ is the rms radius). In general, bunches with
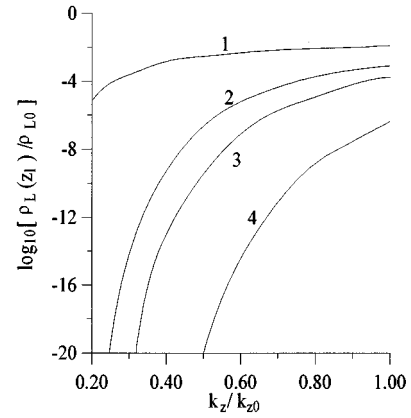
FIG. 4. Normalized line charge density at the longitudinal position where losses occur vs k_z/k_{z0}, for $\varphi_0 = -40°$ and $\Delta\varphi_m = 40°$, $30°$, and $20°$ (curves 1, 2, and 4, respectively), and for $\Delta\varphi_m = 20°$ and $\varphi_0 = -30°$ (curve 3). The aspect ratio in the beam frame is $\gamma_0 z_m / r_m = 2$.

smaller aspect ratios have more significant nonlinearities resulting from the rf field, and slightly higher loss rates with the same k_z/k_{z0}. Figure 5 shows the normalized line charge density as a function of k_z/k_{z0} for a synchronous phase of $\varphi_0 = -40°$, a phase half-width of $\Delta\varphi_m = 30°$, and aspect ratios of 2, 5, and 10 (lines 1, 2, and 3, respectively).

As an example, consider the equipartitioned rf proton linac from Ref. [9], which has a frequency of $\omega_{rf} = 5\times10^9$ s^{-1} and a peak rf electric field of 3.2×10^6 V/m in the high energy structure, particle mass of 1.67×10^{-27} kg and a charge of 1.6×10^{-19} C. The velocity varies from 6.4×10^7 m/s (at 22 MeV with $\gamma_0 \approx 1.02$) to 2.6×10^8 m/s (at 938 MeV with $\gamma_0 = 2$). The normalized rms longitudinal emittance is 1.37×10^{-6} m rad; $\gamma_0\bar{z}$ is 8.7×10^{-4} m at 22 MeV and 3.5×10^{-3} m at 938 MeV. Using $\varphi_0 = -40°$, values for the normalized line charge density are obtained from Fig. 4. At low energy (22 MeV) $\Delta\varphi_m = 20°$; with $k_z/k_{z0} = 0.95$ (a high temperature), Fig. 4 gives a value for the normalized line charge density of about 10^{-7}, resulting in fractional particle losses of about 6×10^{-9}/m along the channel if the beam is perfectly matched and free of oscillations about the synchronous phase.
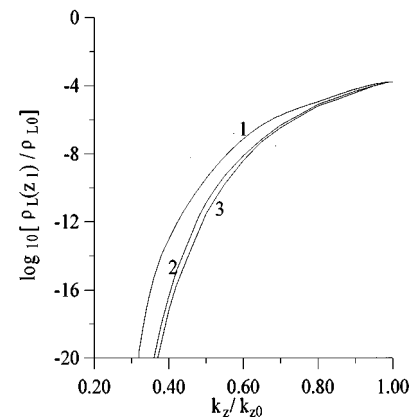
FIG. 5. Normalized line charge density vs k_z/k_{z0} for $\varphi_0 = -30°$ and $\Delta\varphi_m = 20°$ with aspect ratios of $\gamma_0 z_m / r_m = 2$, 5, and 10 (curves 1, 2, and 3, respectively).

IV. CONCLUSION

A mechanism has been described by which current can be lost due to thermal motion during the acceleration and longitudinal focusing of bunched beams in rf linacs. Thermal equilibrium density profiles have been found for a bunched beam focused by the nonlinear forces of the rf bucket in an rf linac, and by the linear transverse focusing of magnetic solenoid or quadrupole lenses. Equations have been derived and numerical results presented for the fractional loss rate of particles from the rf bucket due to thermal motion in the natural tail in the equilibrium distribution. These loss rates are of fundamental importance for rf linacs because they represent the best possible case. Effects such as equipartitioning and mismatch and phase oscillations, which are not included in this paper, can lead to emittance growth, the formation of nonthermal tails (halos), and greater particle losses.

[1] D. Kehne, M. Reiser, and H. Rudd, in *Proceedings of the 1993 Particle Accelerator Conference, Washington, D.C.* (Institute for Electronic and Electrical Engineers, New York, 1993), p. 65.

[2] T. P. Wangler, in *Computational Accelerator Physics, Los Alamos, 1993*, edited by R. Ryne (AIP, New York, 1993), p. 9.

[3] R. L. Gluckstern, Phys. Rev. Lett. **73**, 1247 (1994).

[4] N. Brown and M. Reiser, Phys. Plasmas **2**, 965 (1995).

[5] J. M. Lagniel, Nucl. Instrum. Methods Phys. Res. Sect. A **345**, 46 (1994).

[6] M. Reiser, *Theory and Design of Charged Particle Beams* (Wiley, New York, 1994), Chap. 5.

[7] M. Reiser and N. Brown, Phys. Rev. Lett. **71**, 2911 (1993).

[8] T. P. Wangler, F. W. Guy, and I. Hofmann, in *Proceedings of the 1986 Linear Accelerator Conference, Stanford, CA,* SLAC Report No. 303, 1986, p. 340.

[9] M. Reiser and N. Brown, Phys. Rev. Lett. **74**, 1111 (1995).

[10] M. Reiser, *Theory and Design of Charged Particle Beams* (Ref. [6]), Sec. 3.3.1.

[11] R. L. Spencer, S. N. Rasband, and R. R. Vanfleet, Phys. Fluids B **5**, 4267 (1993).

[12] The temperature in the beam frame (T_b) is related to the temperature in the laboratory frame (T) by $T_b = \gamma T$. The particle number density in the beam frame (n_b) is related to the particle number density in the laboratory frame (n) by $n_b = n/\gamma$. See Ref. [6], Sec. 4.1.